Turkish Journal of Engineering
https://dergipark.org.tr/en/pub/tuje
e-ISSN 2587-1366

Voltage Sensorless Control of Reduced-Order Elementary Super-Lift Luo Converter using Extended Kalman Filter

Ahmet Gani [*1], **Rıdvan Demir** [2]

[1*] *Kayseri University, Electrical and Electronics Engineering, Turkey, ahmetgani@kayseri.edu.tr*
[2] *Kayseri University, Electrical and Electronics Engineering, Turkey, ridvandemir@kayseri.edu.tr*

Cite this study: Gani, A., & Demir, R. (2026). Voltage sensorless control of reduced-order elementary super-lift Luo converter using extended Kalman filter. *Turkish Journal of Engineering, 10*(4), 1229–1236.

https://doi.org/10.31127/tuje.1935755

Keywords
Reduced-Order Elementary Super-Lift Luo Converter
Extended Kalman Filter
Voltage Sensorless Control

Research

Received:22.04.2026
Revised: 25.06.2026
Accepted: 04.07.2026
Published: 15.10.2026

Abstract

Sensorless control approaches can enhance system reliability while reducing sensor cost in dc/dc converters. In this paper, an extended Kalman filter based voltage sensorless control system is proposed to estimate both the input and output voltages of an elementary super-lift Luo converter using a reduced-order model, thereby decreasing the number of sensors. To regulate the output voltage of the elementary super-lift Luo converter, a proportional-integral controller with a reduced number of tuning parameters is designed to minimize steady-state error. The proposed method is evaluated in the MATLAB/Simulink environment under stepwise input/output voltage variations and ramp input voltage variation. The voltage sensorless control system achieves high estimation accuracy with mean absolute error values of 0.2082 V (stepwise input voltage variation), 0.2272 V (stepwise output voltage variation), and 0.1620 V (ramp and stepwise input voltage variation) for the three test scenarios, respectively. In addition, the proportional-integral controller provides a settling time of approximately 55 ms while maintaining negligible steady-state error for all scenarios. The obtained results demonstrate that the proposed voltage sensorless control system provides accurate voltage estimation, robust dynamic performance, and reduced sensor dependency, making it a promising solution for high-performance and cost-effective dc/dc converter applications.

1. Introduction

The switched converters have so far been widely used in different applications such as motor drives and renewable energy systems [1-2].There are different switched dc/dc converter circuit topologies such as buck converter, boost converter, buck-boost converter, Zeta converter, Cuk converter, SEPIC converter, and Luo converter that can be used to increase the input voltage [3].One of the most developed dc/dc switched converters, the elementary super-lift Luo (ESLL) is a new circuit topology for dc/dc conversion based on the super lift method [4], which carries out the dc/dc conversion with geometric progression. In contrast to conventional dc/dc converters, the ESLL converter offers substantial advantages such as high efficiency, low switching element loss, and high voltage gain [5-6]. Other substantial advantages of the ESLL converter are its reduced ripple in both output voltage and input current compared to other conventional dc/dc converters [7-10].The different estimation methods have been used in many engineering applications such as electrical and electronics engineering applications for state and parameter estimation [11-12].Similarly, Kalman filter (KF) based observers have been often employed in the estimation of states and parameters in dc/dc switched power electronic converters for both simulation and real-time implementation[13].Even though there are numerous KF based observers [14-21] to estimate the state and parameter of isolated and non-isolated dc/dc switched power electronic converters, there are a few KF based observers about voltage sensorless control of isolated and non-isolated dc/dc switched power electronic converters. For example, Ref. [14] proposed the extended Kalman filter (EKF) to estimate inductor current, output voltage, and load resistance for the buck

converter topology. Ref. [15] developed and implemented two voltage observers based on EKF for high step-up dc/dc converter, and Ref. [16] designed an observer named steady state hybrid EKF that could estimate the output voltage of an isolated phase-shifted full bridge converter as well as load resistance in real-time for voltage sensorless control. Ref. [17] presented buck converter modeling and estimation of state variables (output voltage and inductor current) in noisy and noiseless conditions using KF. Unlike previous studies, in this paper, the voltage sensorless control system based on EKF which estimates input and output voltages using only the inductor current measurement is proposed for ESLL converter.

A summary of the main innovations of the proposed voltage sensorless control system is presented as follows:

- The EKF not only estimates the input-output voltages but also, inductor current of reduced-order ESLL converter was simultaneously estimated using only the measured inductor current. To the best of the authors' knowledge, this is the first study.
- The proposed control system which was tested under variable input and output voltages produces a robust response with low mean absolute error.
- In order to decrease the sensor count and computational complexity, a reduced-order model of the ESLL converter was considered.
- The proposed output voltage regulator based on proportional-integral (PI) provided a robust scheme for ESLL converter in terms of disturbance inputs and transient response with low steady-state error.

The rest of the present paper is organized as follows: An overview of ESLL converter is presented in Section 2. Section 3 discusses simulation results in detail to verify the effectiveness of the proposed voltage sensorless control system. Finally, Section 4 concludes the study.

2. Overview of ESLL Converter

Introduced by Ref. [22], super lift Luo converter (SLL) topologies offer a higher voltage gain and more effective switch utilization compared to conventional converters, thus causing less switching losses for SLL converter, and creating an output voltage in geometric progression. Depending on the value of voltage gain, different configurations for the main series of the topology are divided into three categories: elementary, re-lift, and triple-lift circuits [23]. Figure 1 shows the circuit structure of ESLL converter which is a third-order system.

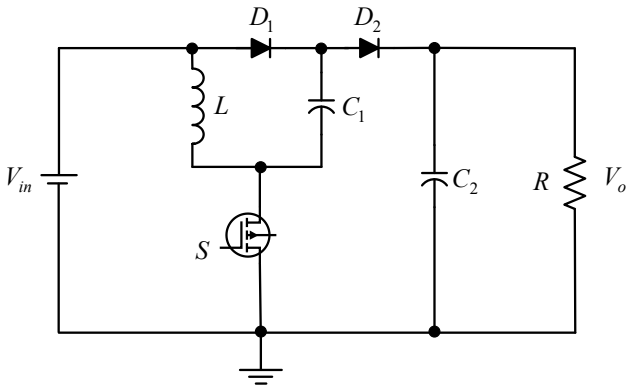


Figure 1. Circuit Structure of ESLL Converter

The ESLL converter is a high-voltage direct current (HVDC) converter that is capable of converting a dc input voltage into the dc output voltage with the same polarity. The voltage increment is performed by controlling the semiconductor switch (S) which is implemented using a MOSFET. The main elements in a circuit diagram of ESLL converter can be listed as two freewheeling diodes (D_1 and D_2), one inductor (L), two capacitors (C_1 and C_2), MOSFET (S). Meanwhile, R is the resistive output load. V_{in} and V_o represent dc input and output voltages, respectively. The ESLL converter achieves a high voltage gain in continuous conduction mode (CCM), as it assumes that all circuit parameters are ideal. Furthermore, pulse-width modulation (PWM) is employed to generate the MOSFET switching signal, enabling effective regulation of the ESLL converter output voltage [24]. The circuit operation of the ESLL converter occurs in two different modes: the switch-on mode and the switch-off mode. The former conducts the switch and diode D_1, while the diode D_2 is off. Meanwhile, a constant level of input voltage charges the capacitor (C_1) and the inductor (L). The capacitor (C_2) supplies energy to the load. Figure 1 (a) shows the ESLL converter in the switch-on mode. Switch-off mode, on the other hand, conducts the diode (D_2), while the switch and diode (D_1) are off. When this mode is active, decreasing inductor current (i_L) provides energy for the capacitor (C_2) and resistive output load (R).

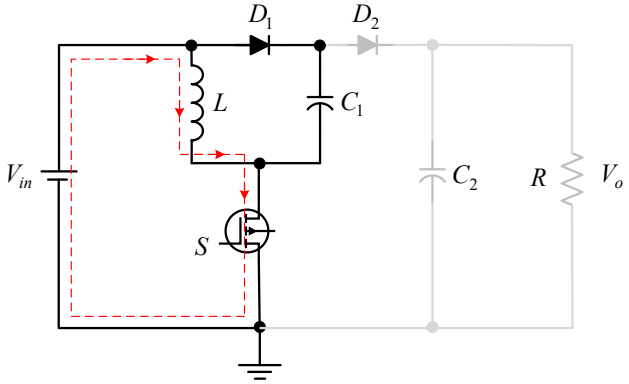


Figure 1 (a): ESLL converter for switch-on condition

At the end, the inductor voltage drops the value of (V_o - $2V_{in}$). ESLL converter in the switch-off mode is shown in Figure 1(b).

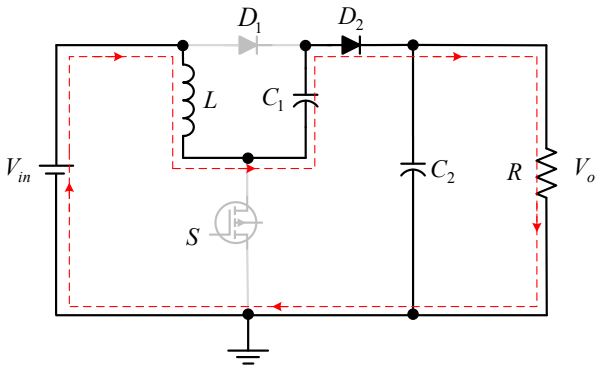


FIGURE 1(b): ESLL converter for switch-off condition

Afterwards, the voltage gain (V_G) of the ESLL converter is calculated as:

$$V_G = \frac{2-d}{1-d} \tag{1}$$

In ESLL converter analysis, Equations (2) and (3) are used to calculate element boundary values based on current and voltage changes in inductors and capacitors, respectively. The variation ratio of the current through *L* inductor can be defined as:

$$\xi = \frac{d(1-d)^2 R}{2(2-d) fL} \tag{2}$$

Generally, ξ is often a very small value, indicating that the ESLL converter operates at CCM normally. The variation ratio voltage across C_2 of the capacitor is calculated via:

$$\delta = \frac{d}{2RfC_2} \tag{3}$$

In a similar way, Equation (3) [25] yields the variation ratio of voltage across (C_1) capacitor. The calculated boundary element values of the ESLL converter are given in Table 1.

Table 1. Selected element values of ESLL converter

DC Input Voltage	V_{in}	60V
Load Resistance	R	150Ω
DC Output Voltage	V_0	300V
Switching Frequency	f	50Khz
Variation ratio of current through inductor *L*	ξ	0.1
Variation ratio of voltage across capacitor $C_{1,2}$	δ	0.02
Capacitor 1	C_1	470µF
Capacitor 2	C_2	470µF
Inductor	L	5mH

2.1. Mathematical Model of ESLL Converter

State equations are used to define the state space model of the ESLL converter. The switch-on and switch-off mode conditions of the ESLL converter are shown in Figure 1 (a) and (b), respectively. The state equations in both modes are given below and finally integrated into state space model.

During on Mode:

$$\frac{di_L}{dt_{on}} = \frac{1}{L} V_{in} \tag{4}$$

$$\frac{dV_0}{dt_{on}} = -\frac{1}{RC_2} V_0 \tag{5}$$

During off Mode:

$$\frac{di_L}{dt_{off}} = \frac{2V_{in}}{L} - \frac{V_0}{L} \tag{6}$$

$$\frac{dV_0}{dt_{off}} = -\frac{1}{C_2} i_L - \frac{1}{RC_2} V_0 \tag{7}$$

Here, t_{on} and t_{off} denote switch-on and switch-off modes of the ESLL converter respectively. In addition, as for (dT) and (1-d) T, d represents the duty cycle, whereas $T = t_{on} + t_{off}$ is the total period of ESLL converter. The state-space model of ESLL converter in matrix forms in switch-on and off-modes can be expressed in Equations (8) and (9), respectively.

$$\dot{x}(t_{on}) = A_1 x(t_{on}) + B_1 V_{in} \tag{8}$$

$$\dot{x}(t_{off}) = A_2 x(t_{off}) + B_2 V_{in} \tag{9}$$

Here, A_1, A_2 and B_1, B_2 are the matrix coefficients. There are two state variables in the reduced-order ESLL converter model: inductor current i_L and capacitor voltage V_{C_2} [26-27]. The continuous-time ESLL converter model is given in the following general reduced-order state-space form:

$$\begin{bmatrix} \dot{i}_L \\ \dot{V}_0 \end{bmatrix} = \begin{bmatrix} 0 & \frac{d-1}{L} \\ \frac{1-d}{C_2} & -\frac{1}{RC_2} \end{bmatrix} \begin{bmatrix} i_L \\ V_0 \end{bmatrix} + \begin{bmatrix} \frac{2-d}{L} \\ 0 \end{bmatrix} V_{in} \tag{10}$$

The general form of ESLL converter model in Equation (10), is discretized by using the forward Euler approximation in Equation (11).

$$\dot{x}(t) \approx \frac{x_{k+1} - x_k}{T} \tag{11}$$

2.2. Voltage Sensorless Control System of Reduced-Order ESLL Converter

The voltage sensorless control system of the ESLL converter is shown in Figure 2 where PI is used as the output voltage regulator and the required output voltage (V_0^{EKF}) is provided by the EKF algorithm. A PI controller is selected owing to its simple structure, low computational complexity, and satisfactory regulation performance.

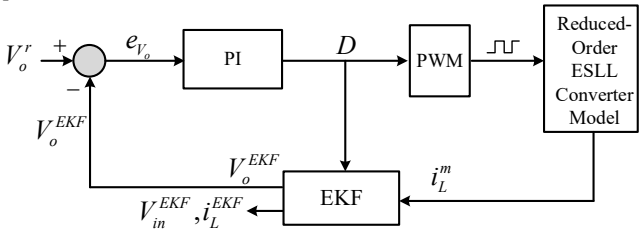


Figure 2. Voltage sensorless control system of ESLL converter based on EKF

As shown clearly in Figure 2, the required output voltage (V_0^{EKF}) is compared with the reference voltage (V_0^r) and generated error (e_{V_0}) voltage that is input to PI. The generated error (e_{V_0}) voltage is mathematically formulated as follows:

$$e_{V_0} = V_0^r - V_0^{EKF} \tag{12}$$

And the control signal (*D*) is applied to the reduced-order ESLL converter model via PWM signal. The control input of the voltage sensorless control system of the reduced-order ESLL converter based on EKF, i.e. control signal (*D*), is mathematically formulated as follows:

$$D = K_p e_{V_0} + K_i \int e_{V_0} \tag{13}$$

Then, the measured inductor current of reduced-order ESLL converter is applied to EKF algorithm and the output-input voltage and inductor current is estimated.

2.2.1. Extended Kalman Filter

To estimate i_L, V_o, and V_{in} simultaneously using EKF, the discretized state equations of the ESLL converter model are given in Equations (14) and (15) which were constructed via Equations (10) and (11). V_{in} is assumed to be in a constant state for the ESLL converter model in the EKF.

$$\begin{bmatrix} i_{L,k+1}^{EKF} \\ V_{0,k+1}^{EKF} \\ V_{in,k+1}^{EKF} \end{bmatrix} = \begin{bmatrix} 1 & \left(\frac{d-1}{L}\right)T & 0 \\ \left(\frac{1-d}{C_2}\right)T & \left(1-\frac{T}{RC_2}\right) & 0 \\ 0 & 0 & 1 \end{bmatrix} \begin{bmatrix} i_{L,k}^{EKF} \\ V_{0,k}^{EKF} \\ V_{in,k}^{EKF} \end{bmatrix} + w \tag{14}$$

$$\begin{bmatrix} i_{L,k} \end{bmatrix} = \begin{bmatrix} 1 & 0 & 0 \end{bmatrix} \begin{bmatrix} i_{L,k}^{EKF} \\ V_{0,k}^{EKF} \\ V_{in,k}^{EKF} \end{bmatrix} + v \tag{15}$$

The conventional equations of the EKF used for the estimations of i_L, V_o, and V_{in} are given below [28].

Linearization

$$\begin{bmatrix} i_{L,k} \end{bmatrix} = \begin{bmatrix} 1 & 0 & 0 \end{bmatrix} \begin{bmatrix} i_{L,k}^{EKF} \\ V_{0,k}^{EKF} \\ V_{in,k}^{EKF} \end{bmatrix} + v \tag{16}$$

Time update

$$\hat{x}_{k+1}^- = f\ (\hat{x}_k^-,\ u_{k+1}) \tag{17}$$

$$P_{k+1}^- = F_{k+1/k}\ P_k\ F_{k+1/k}^T + Q \tag{18}$$

Measurement update

$$K_{k+1} = P_{k+1}^-\ H^T \left[H\ P_{k+1}^- H^T + R \right]^{-1} \tag{19}$$

$$\hat{x}_{k+1} = \hat{x}_{k+1}^- + K_{k+1}\ \left(z_{k+1} - H\ \hat{x}_{k+1}^-\right) \tag{20}$$

$$P_{k+1} = (I - K_{k+1}\ H)\ P_{k+1}^- \tag{21}$$

Here K_{k+1} denotes the Kalman gain, whereas $F_{k+1/k}$ is the function for nonlinear model, P^-_{k+1} and P_{k+1} are priori and posteriori covariance matrices, respectively. Finally, *R* and *Q* represent the covariance matrices for the output and system noise, respectively.

3. Detailed Simulation Results

In this section, the voltage sensorless control based on the EKF estimator and PI output voltage regulator were modeled using the MATLAB/Simulink environment. The inductor current and control signal information of ESLL converter were used by the EKF for the estimation of input and output voltages. To indicate the superiority of the proposed voltage sensorless control system for the ESLL converter, the following scenarios were tested under different operating conditions:

- In the first scenario, the performance of the EKF without V_{in} estimation and control system was employed under stepwise input voltage variation of ESLL converter
- In the second scenario, the performance of the proposed voltage sensorless control system was analyzed under the stepwise output voltage variation of ESLL converter.
- In the third scenario, the performance of the proposed voltage sensorless control system was evaluated under the ramp and stepwise input voltage variation of ESLL converter.

The noise covariance matrices (*Q* and *R*) and the initial prediction error covariance matrix (P_0) of the proposed EKF are critical to the estimation and hence control performance and are chosen by trial-and-error method as in other EKF studies [29]. Additionally, *Q* and *R* are selected as constant and diagonal forms to reduce the computational burden. The values of these matrices are as follows:

$$Q = diag\ \{10^{-2}\ 10^{-2}\ 10^{-1}\} \tag{22}$$

$$P_0 = diag\ \{10\ 10\ 10\} \tag{23}$$

$$R = \{10^{-1}\} \tag{24}$$

The initial values of the output voltage, input voltage, and inductor current estimated by the EKF were selected as zero. In the simulation results, r, m, and EKF superscripts indicate the reference values, the measured quantities, and the estimated quantities by the EKF, respectively. The coefficients of the PI output voltage regulator (K_p and K_i) were determined as 0.01 and 50, respectively, by a trial-and-error method to create the best dynamic system response. In addition, the simulations were carried out in MATLAB/Simulink using the ode23tb solver with a fixed sampling time of 0.1 μs.

3.1 First Scenario

In the first scenario, stepwise input voltage variations were employed to test the estimation performance of the EKF without V_{in} estimation and the output voltage regulation performance of the PI for the ESLL converter. To this aim, V_{in} was suddenly decreased from 60V to 55V at 0.1s and then increased from 55V to 60V at 0.2 s, when the ESLL converter operated under a constant output voltage of 300V. The total simulation time of the first scenario was 0.3s. The simulation results for different stepwise input voltage values obtained from the proposed voltage sensorless control system and PI output voltage regulator with control signal are shown in Figure 3. As can be clearly seen in Figure 3, the variations in V_{in} caused estimation errors, particularly in V_o and i_L estimations and chattering phenomena over output voltage of the ESLL converter, since the EKF assumes that V_{in} was equal to 60V. Therefore, to minimize these estimation errors and chattering phenomena, V_{in} needs to be estimated and updated to EKF.

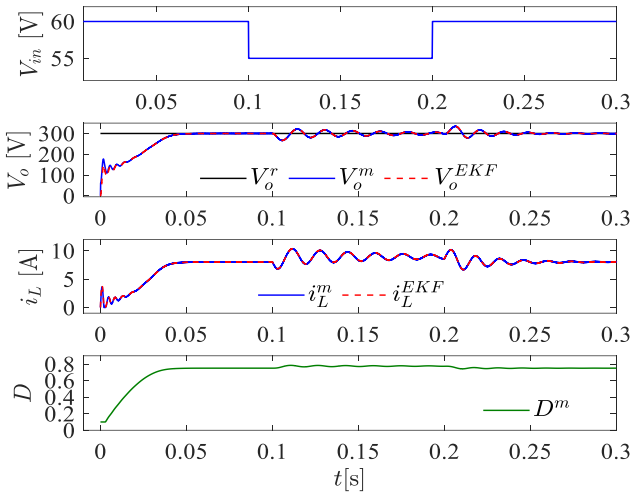


Figure 3. Performance of control system without V_{in} estimation under stepwise input voltage variation of ESLL converter

3.2 Second Scenario

In this scenario, the estimation performance of the proposed voltage sensorless control system and the output voltage regulation performance of PI were analyzed. To this aim, the output voltage of ESLL converter is suddenly decreased from 300V to 250V at 0.1s. Then, the output voltage is abruptly increased from 250V to 300V at 0.2s. Total simulation time of this scenario was 0.3s. The estimation and regulation results for different stepwise output voltage values obtained from proposed voltage sensorless control system and PI are shown in Figure 4.

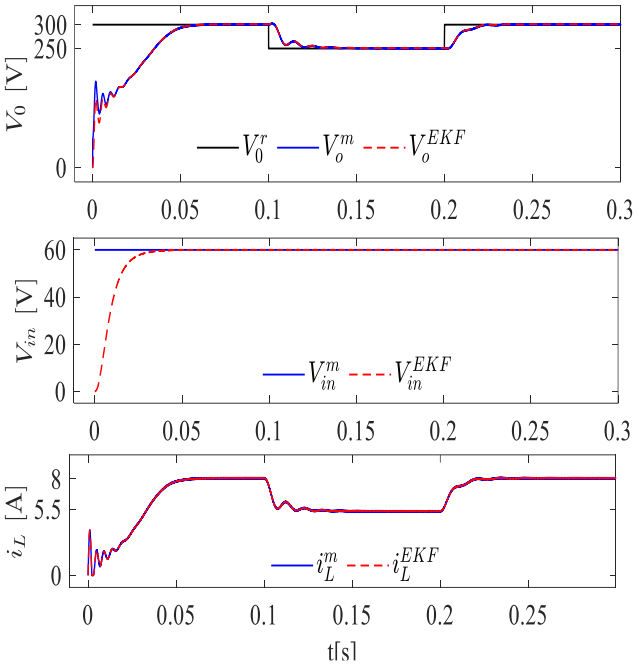


Figure 4. Performance of proposed voltage sensorless control system under stepwise output voltage variation of ESLL converter

It is evident that the settling time value of PI is 55 ms. In addition, the proposed voltage sensorless control system and output voltage regulator based on PI eliminated the influence of the output voltage variations. Indeed, the output voltage of ESLL converter was nearly close to stepwise-generated reference output voltage values after the settling time.

3.3 Third Scenario

In this scenario, the estimation performance of the proposed voltage sensorless control system was evaluated under the ramp and stepwise input voltage changes. To this end, while the ESLL converter operated with the input voltage of 60V, the input voltage was first decreased to 55V linearly at 0.1s. Later the input voltage was suddenly increased from 55V to 60V at 0.4s. Total simulation time of this scenario was 0.6s. The estimation results obtained from the proposed voltage sensorless control system are shown in Figure 5.

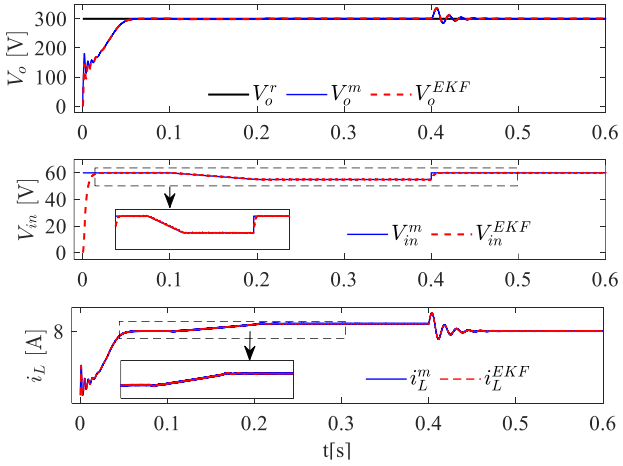


Figure 5. Performance of proposed voltage sensorless control system under ramp and stepwise input voltage variations of ESLL converter

It can be clearly observed that although the output voltage response of the proposed voltage sensorless control system displayed no oscillation against linear variation of input voltage, it displayed a damped oscillation against suddenly change of input voltage in Figure 5. According to the current literature, there are three popular statistical performance indicators that could determine the estimation error of EKF. The *MAE* statistical performance indicator was used for calculation of output voltage estimation error of EKF in this paper and given as follows:

$$MAE = \frac{1}{n}\sum_{i=1}^{n}\left|e_{V_0}\right| \tag{25}$$

The *MAE* values of output voltage estimation error (e_{V_0}) were calculated to evaluate the estimation accuracy of EKF in Table 2 for three scenarios.

Table 2. *MAE* Values of output voltage estimation error (e_{V_0}) for three scenarios

	MAE values
Scenario 1	0.2082 V
Scenario 2	0.2272 V
Scenario 3	0.1620 V

The *MAE* indicator provides a quantitative measure of the EKF estimation accuracy. An *MAE* value close to zero indicates high estimation accuracy. As shown in Table 2, scenario 3 achieved the lowest *MAE* value because the EKF accurately estimated the input voltage, allowing the proposed controller to effectively track the system despite the ramp and step variations in the input voltage.

For an EKF, the steady-state error e_{ssee} is typically defined as the difference between the reference output (or state) and the estimated output (or state) after the transient response has settled. For voltage sensorless control, the steady-state estimation error (e_{ssee}) is:

$$e_{ssee} = \frac{1}{n}\sum_{i=n_s}^{n}\left|e_{V_0}\right| \tag{26}$$

where n_s denotes the beginning of the steady-state region. Table 3 presents the steady-state estimation errors (e_{ssee}) obtained for all three simulation scenarios.

Table 3. The steady-state estimation errors (e_{ssee}) obtained for all three simulation scenarios

	e_{ssee} values
Scenario 1	1.67 V
Scenario 2	0.25 V
Scenario 3	1.53 V

As shown in Table 3, Scenario 2 exhibited the best steady-state estimation performance because the input voltage, which is actively estimated by the EKF, remained constant throughout the simulation. The absence of abrupt input variations allowed the EKF to achieve higher estimation accuracy compared to the other scenarios.

Considering the results obtained from simulation studies as shown in Figures 3-5, the following remarks can be made.

- As shown in Figure 3, when the EKF is configured to estimate only the output voltage (V_0) and inductor current (i_L) while assuming the input voltage (V_{in}) to be constant, changes in the input voltage adversely affect both the estimation accuracy of the EKF and the output voltage regulation performance of the PI controller.
- As depicted in Figure 4, despite the output voltage variations of the ESLL converter, the EKF (which actively estimates V_{in}, V_0, and i_L) effectively maintains a low steady-state estimation error, ensuring the stable operation of the proposed voltage-sensorless control system.
- As seen in Figure 5, despite the input voltage variations of the ESLL converter, the overall performance is quite satisfactory because the proposed EKF accurately estimates all three states (including V_{in}), allowing the PI controller to successfully regulate the system under dynamic conditions.

4. Conclusion

This paper proposed an EKF-based voltage-sensorless control system for an ESLL converter, where the input and output voltages are estimated solely by measuring the inductor current. Simulation results demonstrated that the embedded EKF accurately tracks these voltages under dynamic conditions. This allows the overall control system to effectively handle both input and output voltage variations, yielding low mean absolute errors. Specifically, the steady-state estimation errors for the three simulated scenarios were 0.55%, 0.08%, and 0.51%, respectively.

Compared to conventional sensor-based and single-state estimation approaches, the proposed method achieves superior estimation accuracy with reduced sensor dependency and improved robustness. Therefore, it is safe to conclude that this strategy paves the way for the development of more robust and high-performance sensorless control policies for the ESLL converter, as well as other dc/dc converter topologies.

In future studies, we plan to experimentally validate the performance of the proposed control system on real converter hardware. Furthermore, we aim to investigate fault diagnosis and fault-tolerant control methods for dc/dc converters.

Author contributions

Ahmet Gani: Conceptualization, Methodology, Field study and Writing-Original draft preparation.

Rıdvan Demir: Visualization, Investigation, Software and Validation.

Conflicts of interest

The authors declare no conflicts of interest.

References

1. Gülbudak, O., & Gökdağ, M. (2022). Performance evaluation of model predictive control method for neutral point clamped inverter. Turkish Journal of Engineering, 6(3), 245-250. https://doi.org/10.31127/tuje.962857.
2. Keçecioğlu, O.F., Gani, A., & Sekkeli, M., (2021). Improved hybrid intelligent controller design for MPPT of stand-alone PV System. Turkish Journal of Engineering, 5(1), 20-28. https://doi.org/10.31127/tuje.652229.
3. Gauswami, A., & Shah, H. (2026). A comparative simulation–hardware co-validation framework for SEPIC and full-bridge DC–DC converters in electric vehicle battery charging via dSPACE DS1104. Turkish Journal of Engineering, 10(2), 534-547. https://doi.org/10.31127/tuje.1828170.
4. Gani, A., (2025). Advanced controller design based on interval type-2 fuzzy neural network for elementary super-lift Luo converter. Transactions of the Institute of Measurement and Control, 47(10), 1953-1963. https://doi.org/10.1177/01423312241275 76.
5. Gani, A., (2021). Improving dynamic efficiency of photovoltaic generation systems using adaptive type-2 fuzzy neural network via EN 50530 test procedure. International Journal of Circuit Theory and Applications, 49(11), 3922–3940. https://doi.org/10.1002/cta.3139.
6. Gani, A., (2023). PD-type-2 fuzzy neural network based control of a super-lift Luo converter designed for sustainable future energy applications. In: Kahraman, C., Sari, I.U., Oztaysi, B., Cebi, S., Cevik Onar, S., Tolga, A.Ç. (eds) Intelligent and Fuzzy Systems. INFUS 2023. Lecture Notes in Networks and Systems, vol 758. Springer, Cham.https://doi.org/10.1007/978-3-031-39774-5_62.
7. Gani, A., (2023). PEM yakıt hücresi ömrünü uzatmaya yönelik temel seri pozitif süper gerilim yükseltmeli Luo çevirici tasarımı. Erciyes Üniversitesi Fen Bilimleri Enstitüsü Fen Bilimleri Dergisi, 39(3), 403-416. https://izlik.org/JA84NU86LC.
8. Toren, M., Kaba, B., & Öztürk, G., (2025). Performance comparison of boost and super-lift Luo converters in solar energy systems using fuzzy logic based MPPT control. Pamukkale Üniversitesi Mühendislik Bilimleri Dergisi, https://doi.org/10.65206/pajes.92724.
9. Garg, M.M., Pathak, M.K., & Behera, L., Dynamic modeling of a non-ideal DC-DC positive output elementary super-lift Luo converter, International Conference on Technological Advancements in Power and Energy *(TAP Energy)*, Kollam, India, 2017, pp. 1-6, https://doi.org/10.1109/TAPENERGY.2017.8397296.
10. Kaba, B., Tören, M., & Şahin, M.E., (2026). Investigation of the super-lift Luo converter controlled with PI and SM control for electric vehicle battery sources. Journal of Engineering Research.14(2),1782-1791. https://doi.org/10.1016/j.jer.2026.01.008.
11. Kamarudin, M. R., Mispan, M. S., Zainudin, M. N. S., & Sofian, H., (2026). Reservoir spiking neural networks for accurate state-of-charge estimation in battery management systems. Turkish Journal of Engineering, 10(2), 407-417. https://doi.org/10.31127/tuje.1804828.
12. Chaudhari, T., (2026). State of charge estimation of sustainable low emission electrochemical energy storage systems. Turkish Journal of Engineering, 10(2), 689-706. https://doi.org/10.31127/tuje.1841528.
13. Bulut, Y. (2011). Applied Kalman filter theory (Doctoral dissertation, Northeastern University). Northeastern University Repository.
14. Candan, M. Y., & Ankarali, M.M. (2020). Extended Kalman filter based state and parameter estimation method for a buck converter operating in a wide load range. In 2020 IEEE Energy Conversion Congress and Exposition (ECCE) (pp. 3238–3244). IEEE. https://doi.org/10.1109/ECCE44975.2020.9235695.
15. Haadi, K., Rajaei, A., Shahparasti, M., & Rahideh, A. (2020). Sensorless voltage observer for a current-fed high step-up DC–DC converter using extended Kalman filter. Electronics, *9*(12), 2066. https://doi.org/10.3390/electronics9122066.
16. Candan, M. Y., & Ankarali, M. M. (2023). Steady-state hybrid extended Kalman filter based sensorless voltage controller for a phase-shifted full-bridge converter. IET Power Electronics, *16*(1),53–63. https://doi.org/10.1049/pel2.12362.
17. Eker, K., Çetinceviz, Y., Şehirli, E., & Erken, F. (2022). State estimation of buck converter by using Kalman filter. In 2022 Global Energy Conference (GEC) (pp. 402–407). IEEE. https://doi.org/10.1109/GEC55014.2022.9986519.

18. Zhang, Q., Tong, Q., & Zhang, H. (2014). An inductor current observer based on improved EKF for DC/DC converter. In International Symposium on Computer Consumer and Control (pp.892–895).IEEE. https://doi.org/10.1109/IS3C.2014.235.
19. Cimini, G., Ippoliti, G., Orlando, G., Longhi, S., & Miceli, R. (2017). A unified observer for robust sensorless control of DC–DC converters. Control Engineering Practice, 61, 21–27. https://doi.org/10.1016/j.conengprac.2017.01.012.
20. Tong, Q., Chen, C., Zhang, Q., & Zou, X. (2015). A sensorless predictive current controlled boost converter by using an EKF with load variation effect elimination function. Sensors, 15(5), 9986–10003. https://doi.org/10.3390/s150509986.
21. Ahmeid, M., Armstrong, M., Gadoue, S., Al-Greer, M., & Missailidis, P. (2017). Real-time parameter estimation of DC–DC converters using a self-tuned Kalman filter. IEEE Transactions on Power Electronics, 32(7), 5666–5674. https://doi.org/10.1109/TPEL.2016.2606417.
22. Luo, F. L., & Ye, H. (2003). Positive output super-lift converters. IEEE Transactions on Power Electronics, 18(1), 105–113. https://doi.org/10.1109/TPEL.2002.807198.
23. Gani, A., & Uçar, İ. (2024). Enhanced Control of polymer electrolyte membrane fuel cell fed Basic series positive super voltage lift Luo converter using interval type-2 fuzzy logic. Gazi Üniversitesi Fen Bilimleri Dergisi Part C: Tasarım Ve Teknoloji, 12(2), 457-467. https://doi.org/10.29109/gujsc.1433379.
24. Luo, F. L., Ye, H., & Rashid, M., (2002). Super-lift Luo-converters. In Proceedings of the IEEE 33rd Annual Power Electronics Specialists Conference (Vol. 2, pp. 425–430). IEEE. https://doi.org/10.1109/PSEC.2002.1022490.
25. Luo, F. L., & Ye, H. (2003). Advanced DC/DC converters. CRC Press. https://doi.org/10.1201/9780203492925.
26. Femi, R., Sree Renga Raja, T., & Shenbagalakshmi, R. (2021). A positive output-super lift Luo converter fed brushless DC motor drive using alternative energy sources. International Transactions on Electrical Energy Systems, 31(2), e12740.https://doi.org/10.1002/2050-7038.12740.
27. Glady, J. B. P., & Manjunath, K. (2019). Analysis-intelligent design and simulation of improved state-space modelling for control of Luo converter. Computers & Electrical Engineering, 75,230–244. https://doi.org/10.1016/j.compeleceng.2017.11.010.
28. Demir, R., (2023). Robust stator flux and load torque estimations for induction motor drives with EKF-based observer. Electrical Engineering, 105(1), 551–562. https://doi.org/10.1007/s00202-022-01717-y.
29. Yildiz R., Demir R., and Barut M., (2023).Online estimations for electrical and mechanical parameters of the induction motor by extended Kalman filter, Transactions of the Institute of Measurement and Control 45(14), 2725-2738, https://doi.org/10.1177/01423312231160582.

© Author(s) 2026. This work is distributed under https://creativecommons.org/licenses/by-sa/4.0/